Zhao, O., Gardner, L. and Young, B. (2019). Finite element modelling and design of stainless steel SHS and RHS beam-columns under moment gradients. Thin-walled Structures. 134:220–232.

Finite element modelling and design of stainless steel SHS and RHS beam-columns under moment gradients

Ou Zhao [*a], Leroy Gardner [b], Ben Young [c]

[a] School of Civil and Environmental Engineering, Nanyang Technological University, Singapore

[b] Dept. of Civil and Environmental Engineering, Imperial College London, London, UK

[c] Dept. of Civil Engineering, The University of Hong Kong, Hong Kong, China

[*] Corresponding author, Phone: +65 6790 6934

Email: ou.zhao@ntu.edu.sg

Abstract

Structural design formulae for beam-columns require accurate end points (i.e. accurate resistance predictions for pure compression and pure bending), should be of suitable form to capture the interaction between the different components of loading and should take due account of the influence of a moment gradient along the member length. However, existing design rules for stainless steel beam-columns do not fully capture the interaction responses observed in experiments and numerical simulations, and are often tied to inaccurate end points; the adopted equivalent uniform moment factors can also be unconservative in the case of high moment gradients. As a consequence, previous comparisons of stainless steel beam-column experimental and finite element results with codified strength predictions have often revealed a rather high degree of scatter. This prompted the present research, to develop improved design proposals for stainless steel square hollow section (SHS) and rectangular hollow section (RHS) beam-columns under moment gradients. To this end, revised design approaches are proposed firstly through the derivation of more accurate design interaction curves for stainless steel SHS and RHS beam-columns under uniform bending moment and then through the employment of more suitable equivalent uniform moment factors, underpinned by and validated against over 1500 test and numerical data points. The new design approaches are shown to lead to improved (safe-sided, accurate and consistent) resistance predictions for stainless steel SHS and RHS beam-columns under moment gradients over the current codified design rules. Finally, statistical analyses are performed to demonstrate the reliability of the proposed approaches, according to the requirements specified in EN 1990.

1. Introduction

Beam-column structural members simultaneously transmit bending moments and axial forces, and the failure modes thus involve combined bending (leading to in-plane or out-of-plane deformations) and column buckling. Extensive research has been performed to study the buckling behaviour of carbon steel beam-column members and to derive accurate design interaction formulae in the last decade [1–8]. However, with regards to beam-columns made of stainless steel, the corresponding experimental and numerical investigations and developments in design guidance are rather limited; a brief summary of these studies is presented herein. Tajia and Salmi [9] experimentally examined the global buckling behaviour of austenitic stainless steel SHS and RHS beam-columns under the combined actions of compression and uniform first-order bending moment, while corresponding tests on normal duplex and lean duplex stainless steel SHS and RHS beam-columns were reported by Lui et al. [10] and Huang and Young [11], respectively. Zhao et al. [12] and Arrayago et al. [13] also carried out beam-column tests on ferritic stainless steel SHS and RHS. The global stability of austenitic stainless steel circular hollow section (CHS) beam-columns under compression and uniform first-order bending moment was investigated by Zhao et al. [14], based on a comprehensive testing and finite element simulation programme. Experiments on ferritic stainless steel SHS and RHS beam-columns under unequal end moments were performed by Zhao et al. [15] to study their interaction buckling behaviour under moment gradients. Following comparisons against these experimental and numerical data, it has generally been found [9–15] that the codified beam-column design interaction curves result in rather inaccurate and scattered strength predictions. Greiner and Kettler [16] and Lopes et al. [17] proposed revised stainless steel beam-column design interaction curves, which led to improved strength predictions, but were hindered by their reliance on inaccurate end points, based on the EN 1993-1-4 [18] column buckling strengths and member bending resistances [19,20]. Zhao et al. [19,20] recently derived a new set of interaction factors for stainless steel tubular section (SHS, RHS and CHS) beam-column members under uniform bending moment, on the basis of more accurate end point values, with the column buckling end point (i.e. column buckling strength) calculated from the revised column buckling curves proposed by Afshan et al. [21] and the bending end point (i.e. bending moment capacity) determined from the deformation-based continuous strength method [22–26]. The proposals have been shown to yield accurate, consistent and safe strength predictions for stainless steel tubular beam-columns under compression and uniform bending moment [19,20].

The focus of the present paper is on the finite element simulation and design of stainless steel non-slender SHS and RHS beam-columns under moment gradients. An existing experimental study [15] is firstly summarised, after which a numerical modelling programme, comprising a validation study to replicate the tests and a numerical parametric study to generate additional data, is described. The obtained test and numerical results are employed to investigate the buckling behaviour of stainless steel SHS and RHS beam-columns under moment gradients, and to assess the accuracy of the existing design provisions in the European code EN 1993-1-4 [18], American specification SEI/ASCE-8 [27] and Australian/New Zealand standard AS/NZS 4673 [28]. The limitations of these codified beam-column design rules are highlighted, and new design proposals are then made to overcome the identified shortcomings. The accuracy and reliability of the new proposals are assessed, based on over 1500 test and numerical results.

2. Review of existing experimental data

The only previous experimental study of the global stability of stainless steel beam-columns under moment gradients was reported by the authors in Zhao et al. [15]. The beam-column tests were conducted on two ferritic stainless steel (Grade 1.4003) cross-sections – SHS 60×60×3 and RHS 100×40×2. For each cross-section size, two nominal member lengths were used, while for each member length, six beam-column tests were performed under varying end moment ratios, resulting in a range of moment gradients along the member length being examined. The end moment ratio ψ is defined as the ratio of the smaller to the larger end moments, with positive and negative values indicating single and double curvature bending, respectively, following the convention used in EN 1993-1-1 [29]. The beam-column tests were carried out through the use of knife-edges to provide pin-ended boundary conditions, with the experimental rig shown in Fig. 1. For each test series (i.e. specimens with the same nominal member length), the loading eccentricities were fixed to the same nominal value at the bottom ends of the specimens, but varied at the top ends, in order to achieve a range of end moment ratios between -1.0 and 1.0.

Table 1 presents a summary of the key obtained experimental results for each beam-column specimen [15], where L_{cr} is the effective length of the specimen, measured between the top and bottom knife-edges, $\bar{\lambda}$ is the corresponding non-dimensional member slenderness [29], e_0 is the initial loading eccentricity at the bottom end of the specimen, ψ is the end moment ratio, $N_{u,test}$ is the failure load, and $M_{u,b}=N_{u,test}e_0$ and $M_{u,t}=N_{u,test}e_0\psi$ are respectively the failure moments at the bottom end and top end of the specimen. The utilised designation system for the test series begins with the nominal dimension of the adopted SHS (or RHS), followed by the axis of buckling, and ends with the nominal length of the beam-column specimen (in mm), e.g., SHS 60×60×3-1200. The beam-column specimen ID within each test series consists of a number and a letter, e.g., 2B, with the numbers from '1' to '4' indicating the different test series and the letters A–F identifying the varying end moment ratios used within each test series. Typical failure modes for specimens from the SHS 60×60×3-600 test series (i.e. SHS 60×60×3 beam-column specimens with the same nominal member length of 600 mm) are shown in Fig. 2, showing that the location of the critical cross-section migrates from the end of the specimen to the member mid-height, as ψ varies from -1.0 (corresponding to an antisymmetric triangular first-order moment distribution) to 1.0 (representing a uniform first-order moment distribution).

3. Numerical modelling

A comprehensive numerical modelling study, conducted by means of the finite element (FE) analysis package ABAQUS [30], is presented in this section. The numerical models were firstly developed and validated against the test results reported in [15] and then utilised to carry out numerical parametric studies to generate further results over a broader range of stainless steel grades, cross-section geometric proportions, member lengths, loading eccentricities and end moment ratios. The derived FE results, together with the experimental data, were utilised to access the accuracy of the existing codified interaction formulae for the design of stainless steel SHS and RHS beam-columns under moment gradients and to develop improved design provisions.

In the present finite element modelling study, the four-noded shell element S4R [30] was adopted; this element type has been extensively and successfully employed in previous FE simulation of stainless steel thin-walled beam-column elements [12,14,19,31–34]. The element size for the flat portions of the FE models was equal to the material thickness, while the curved corner parts were discretised by four elements. The measured engineering material properties [15] were firstly converted into the format of true stress and true plastic strain, and then inputted into ABAQUS [30]. Stainless steel tubular (closed) section structural members are generally cold-rolled, and previous experimental and numerical studies [31,35] verified that both the corner regions and the adjacent flat regions beyond the corners by a distance of two times the cross-section thickness experience a similar level of enhancement in material strength during the cold-rolling process, and exhibit similar material characteristics. Thus, the measured corner material properties were assigned to both of the aforementioned regions in the numerical models, while the remainder of the numerical models was assigned with the flat material properties. Membrane and bending residual stresses were introduced into the stainless steel SHS and RHS specimens during the fabrication (cold-forming and seam welding) process. However, residual stresses were not explicitly modelled in the present numerical simulation, principally owing to the fact that (i) the membrane residual stresses are negligible in cold-formed and seam-welded stainless steel tubular profiles [36–38], and (ii) the effect of the more dominant bending residual stresses is inherently presented in the measured material properties upon straightening of the tensile coupons during material testing [36–38].

The nodes of each (top and bottom) end section of the beam-column models were coupled to an eccentric reference point, with the eccentricity equal to the corresponding value employed in the beam-column tests. The applied boundary conditions allowed the top reference point to rotate freely about the buckling axis and the bottom reference point to rotate about the same buckling axis as well as translate longitudinally, to simulate the experimental pin-ended boundary conditions. An axial compressive load was then applied to the numerical models through the bottom reference point, which resulted in the application of the combined actions of axial compression force and unequal end moments to the beam-column members.

Initial geometric imperfections were incorporated into the FE models in order to accurately simulate the physical responses observed in the experiments. The initial global geometric imperfection distribution was taken as a half-sine wave along the model length, while the initial local imperfection pattern was assumed to be in the form of the lowest elastic local buckling mode shape under the combined loading. Two local imperfection amplitudes and three global imperfection amplitudes were adopted to factor the respective imperfection shapes, enabling the sensitivity of the developed numerical models to different levels of imperfections to be studied. The two considered local imperfection values were (i) the measured amplitude ω_0 [15] and (ii) the amplitude calculated from the predictive model $\omega_{D\&W}$, as defined by Eq. (1) [31,39], in which $\sigma_{0.2}$ is the material 0.2% proof stress (yield stress), $\sigma_{cr,min}$ and t are the elastic critical buckling stress and thickness of the most slender plate element of the SHS (or RHS). The three considered amplitudes for the initial global geometric imperfection were the measured value ω_g [15] and 1/1000 and 1/1500 of the effective length of the specimen. Finally, static Riks analysis, accounting for both material and geometric nonlinearities, was conducted to simulate the full experimental response of each beam-column specimen.

$$\omega_{D\&W} = 0.023\left(\frac{\sigma_{0.2}}{\sigma_{cr,\min}}\right)t \tag{1}$$

The accuracy of the developed FE models was evaluated through comparing the numerical failure loads, load–lateral deflection curves and failure modes with the corresponding experimental results [15]. Table 2 reports the FE to test failure load ratios, indicating that all the six examined combinations of initial global and local imperfection values yield good agreement between the experimental and numerical failure loads. Fig. 3 displays the test and FE load–lateral deflection curves for a typical specimen SHS 60×60×3-600-3C, where the full experimental response is shown to be well simulated by the numerical model. Excellent agreement is also obtained when comparisons are made between the experimental and FE failure modes, as displayed in Fig. 2. In summary, the developed numerical models are found to be capable of simulating the experiments, and are thus considered to be validated.

Parametric studies were then performed, using the validated FE models, to generate more data over a broader range of stainless steel grades (austenitic, duplex and ferritic), cross-section proportions, member lengths, loading eccentricities and end moment ratios. In the present numerical parametric studies, the utilised material properties for the ferritic stainless steel sections were taken from the tensile coupon tests on the SHS 60×60×3 [15], while the material properties for the austenitic and duplex stainless steel sections were taken from previous beam-column specimens tested under uniform bending moment [11,40]. Table 3 presents the employed material properties for the three stainless steel grades, including the

Young's modulus E, the 0.2% and 1.0% proof stresses $\sigma_{0.2}$ and $\sigma_{1.0}$, the ultimate tensile stress σ_u, and the exponents employed in the Ramberg–Osgood (R–O) material model n, $n'_{0.2,1.0}$ and $n'_{0.2,u}$ [41–45]. The initial local imperfection values were predicted from Eq. (1) [31,39], while the amplitudes of the initial global imperfection were taken as $L_{cr}/1000$, which is consistent with previous studies [12,14,19]. Regarding the cross-section geometric properties, the outer section widths were fixed at 100 mm, while the outer section depths were varied between 100 mm and 200 mm, which resulted in a range of cross-section aspect ratios from 1.0 to 2.0; the internal corner radii of the modelled SHS and RHS were set equal to the corresponding material thicknesses, which ranged from 4 mm to 10 mm. The modelled SHS and RHS covered all three non-slender cross-section classes (i.e. Class 1–3), according to the classification limits specified in EN 1993-1-4 [18]. The model lengths were varied, in order to provide a wide spectrum of member non-dimensional slenderness $\bar{\lambda}$ between 0.2 and 3.0. The initial loading eccentricities at the bottom ends of the FE models ranged from 5 mm to 350 mm, and the end moment ratios varied between -1.0 and 1.0, in increments of 0.1, leading to a wide range of loading combinations and moment gradients being examined. In total, 1500 numerical parametric results were generated, with 500 for each stainless steel grade.

4. Established codified design approaches

The established design provisions for stainless steel SHS and RHS beam-columns under the combined actions of compression and moment gradients, given in EN 1993-1-4 [18], SEI/ASCE-8 [27] and AS/NZS 4673 [28], are discussed, with their limitations highlighted, in this section. The accuracy of the current design codes is then assessed by comparing the experimentally and numerically derived beam-column failure loads with the unfactored failure load predictions $N_u/N_{u,pred}$, as presented in Table 4. Note that ratios of $N_u/N_{u,pred}$ greater than unity indicate safe-sided capacity predictions.

The design interaction formulae for stainless steel SHS and RHS beam-columns under moment gradients in the three considered codes follow the same format, as shown in Eq. (2), in which N_{Ed} and M_{Ed} are the applied (design) axial force and maximum first-order bending moment, respectively, $N_{b,Rd}$ is the column flexural buckling strength, $M_{b,Rd}$ is the member bending moment resistance, taken as the corresponding cross-section bending moment capacity $M_{c,Rd}$ for SHS and RHS structural members which are not susceptible to lateral torsional buckling (provided that the cross-section height-to-width ratio is not too high), k is the interaction factor for beam-columns under uniform first-order bending moment, which takes into account both the beneficial effect of the spread of plasticity within the cross-section and the detrimental geometric second-order effect on the member stability, and C_m is the equivalent uniform moment factor, employed to account for the additional favourable effect of the non-uniform bending moment distribution on the beam-column global buckling behaviour. There are, however, differences between the three codes in the calculation of the column buckling strengths $N_{b,Rd}$ and cross-section bending moment capacities $M_{c,Rd}$, which act as the end points of the stainless steel beam-column design interaction curve defined by Eq. (2), and the interaction factors k and the equivalent uniform moment factor C_m, which determine the general shape of the interaction curve.

$$\frac{N_{Ed}}{N_{b,Rd}} + C_m k \frac{M_{Ed}}{M_{b,Rd}} \leq 1 \qquad (2)$$

For the calculation of column flexural buckling resistance, EN 1993-1-4 [18] defines a series of buckling curves for various types of open and hollow section members; the corresponding imperfection factors and limiting slendernesses are given in Table 5.3 of EN 1993-1-4 [18].

The American specification SEI/ASCE-8 [27] adopts the tangent modulus method to calculate the reduced stiffness at the buckling stress, in order to account for the effect of the rounded (nonlinear) material stress–strain response of stainless steel on column buckling. AS/NZS 4673 [28] adopts the same tangent modulus method as SEI/ASCE-8 [27], but also provides an alternative explicit method [46] for the predictions of column flexural buckling strengths, as given in Clause 3.4.2 of AS/NZS 4673 [28]. Previous studies [12,14,15,19] on stainless steel columns have indicated that both the EN 1993-1-4 buckling curves and the SEI/ASCE-8 tangent modulus approach often lead to predictions of column buckling strengths that lie on the unsafe side, while the explicit method used in AS/NZS 4673 [28] generally yields good, if slightly conservative strength predictions. With regards to cross-sectional bending moment capacity, EN 1993-1-4 [18] prescribes the use of the plastic $M_{pl,Rd}$ and elastic $M_{el,Rd}$ moment resistances for Class 1 (or 2) and Class 3 cross-sections, respectively, while SEI/ASCE-8 [27] and AS/NZS 4673 [28] adopt the inelastic reserve method for predicting the cross-sectional bending capacities. All of these methods, however, neglect strain hardening and use the 0.2% proof stress (yield stress) as the design stress, and have thus been found by many researchers [12,19,47,48] to yield unduly conservative bending moment resistance predictions when compared against bending test results. The interaction factors for stainless steel beam-columns under uniform first-order bending moment, adopted in the current versions of EN 1993-1-4 [18], SEI/ASCE-8 [27] and AS/NZS 4673 [28] (k_{EC3}, k_{ASCE} and $k_{AS/NZS}$, respectively), are given by Eqs (3) and (4). Owing to the limitations of the end points described above, these interaction factors, particularly those adopted in EN 1993-1-4 [18], not only represent the interaction effects, but also compensate, to some extent, for the difference between the actual and adopted end point values [16,19].

$$1.2 \leq k_{EC3} = 1 + 2\left(\bar{\lambda} - 0.5\right)\frac{N_{Ed}}{N_{b,Rd}} \leq 1.2 + 2\frac{N_{Ed}}{N_{b,Rd}} \tag{3}$$

$$k_{ASCE} = k_{AS/NZS} = 1 - \frac{N_{Ed}}{N_{cr}} \tag{4}$$

Following comparisons against the experimental and numerical results, Zhao et al. [12,14,19] concluded that the existing international design codes yield rather scattered resistance predictions for stainless steel tubular beam-columns under uniform bending moment. Specifically, EN 1993-1-4 [18] and SEI/ASCE-8 [27] often yield optimistic resistance predictions for stainless steel tubular beam-columns with high levels of axial compression, but conservative predicted strengths for beam-columns where bending effects are more dominant. AS/NZS 4673 [28] was found to result in an increased level of design accuracy, principally owing to the improvement in the predictions of the column buckling end point, but the level of scatter was still similar to that of EN 1993-1-4 [18] and SEI/ASCE-8 [27].

The equivalent uniform moment factor is employed to account for the favourable effect of non-uniform bending moment distributions on beam-column stability. For the design of stainless beam-columns subjected to unequal end moments (leading to a moment gradient along the member length), the corresponding equivalent uniform moment factors employed in SEI/ASCE-8 [27] and AS/NZS 4673 [28] ($C_{m,ASCE}$ and $C_{m,AS/NZS}$, respectively) are given by Eq. (5). EN 1993-1-4 [18], however, neglects this beneficial effect in the design of stainless steel beam-columns under non-uniform bending moments, and thus $C_{m,EC3}$ is equal to unity, as shown in Eq. (6).

$$C_{m,ASCE} = C_{m,AS/NZS} = 0.6 + 0.4\psi \tag{5}$$

$$C_{m,EC3} = 1.0 \tag{6}$$

The experimental and numerical results were compared with the failure loads predicted from the three considered international design standards. The results of the comparisons, as presented in Table 4(a)–4(c), show that EN 1993-1-4 [18] yields the most inaccurate capacity predictions for stainless steel SHS and RHS beam-columns under moment gradients, and the level of conservatism increases as ψ varies from 1.0 to -1.0, owing principally to the neglect of the beneficial effect of the non-uniform bending moment distributions on the global stability of beam-columns. This can also be seen from Figs 4–6, in which the experimental (or numerical) to EC3 predicted failure load ratio is plotted against the end moment ratio. The American specification [27] is found to yield accurate capacity predictions on average, but many predictions lie on the unsafe side, particularly for beam-columns under high levels of moment gradient, as shown in Tables 4(a)–4(c) and Figs 4–6. The over-predicted capacities result mainly from the adopted column buckling end point of the design interaction curve, and from the employed equivalent uniform moment factor, which appears to overestimate the favourable effect of moment gradient on the global stability of stainless steel beam-columns. Compared to SEI/ASCE-8 [27], AS/NZS 4673 [28] is generally shown to result in slightly less precise strength predictions, but with fewer on the unsafe side and with a similar level of scatter.

5. Derivation of improved beam-column design approaches

5.1 General

The established codified design interaction formulae for stainless steel beam-columns under moment gradients, as discussed in Section 4, were developed through the use of the corresponding design formulae for beam-column members under uniform bending moment but with an additional equivalent uniform moment factor to take into account the favourable effect of the non-uniform moment distribution on the beam-column stability. Similarly, improved design approaches are sought herein firstly through the derivation of more accurate design interaction curves for beam-columns under uniform bending moment and then through the employment of more suitable equivalent uniform moment factors.

5.2 New design formulae for stainless steel beam-columns under uniform bending moment

The existing codified design interaction curves for stainless steel beam-columns under uniform bending moment suffer from (i) inaccurate end points, where the compression end points (i.e. column buckling strengths) are often overestimated, while the bending end points are unduly conservative owing to the lack of consideration of the material strain hardening of stainless steel, and (ii) inaccurate interaction factors, which not only represent the interaction between compression and bending, but also compensate for the difference between the actual and adopted end point values [16,19]. Improved design approaches for stainless steel tubular section (SHS, RHS and CHS) beam-columns have been proposed by the authors [19,20], through the employment of more precise end points and the derivation of more efficient interaction curves, anchored to the new end points. A brief summary of the derivation of the new design approaches for stainless steel SHS and RHS beam-columns under uniform bending moment is presented herein.

In the proposed approach [19], the compression end point (i.e. the column buckling strength) is determined based on the revised buckling curves recommended by Afshan et al. [21]. With regards to the design of stainless steel SHS and RHS columns, the revised buckling curves, as depicted in Fig. 7, use the same imperfection factor α=0.49 as EN 1993-1-4 [18], but with lower limiting slendernesses $\bar{\lambda}_0$ of 0.2 and 0.3 for ferritic stainless steel and austenitic and duplex stainless steels, respectively, in comparison with the EC3 limiting slenderness that is equal to 0.4. The revised buckling curves were shown to lead to more accurate and consistent column flexural buckling capacity predictions [19,21], compared to the current buckling curve defined in EN 1993-1-4 [18], which often yields over-predicted resistances.

The bending end point is determined through the use of the continuous strength method (CSM), which takes into account strain hardening in the calculation of stainless steel cross-sectional resistances. The application of the CSM firstly requires the use of 'base curves' to identify the cross-section limiting strain ε_{csm}, and then the use of an elastic, linear hardening material model to consider strain hardening. The base curves are given by Eq. (7) and Eq. (8) for non-slender plated sections and slender plated sections, respectively, where ε_y is the yield strain, defined as $\varepsilon_y=\sigma_{0.2}/E$, and $\bar{\lambda}_p = \sqrt{\sigma_{0.2} / \sigma_{cr}}$ is the cross-section slenderness, in which σ_{cr} is the elastic critical buckling stress of the full cross-section in bending, and determined herein by the finite strip software CUFSM [49].

$$\frac{\varepsilon_{csm}}{\varepsilon_y} = \frac{0.25}{\bar{\lambda}_p^{\,3.6}} \text{ but } \le \min\left(15, \frac{C_1\varepsilon_u}{\varepsilon_y}\right), \quad \text{for } \bar{\lambda}_p \le 0.68 \tag{7}$$

$$\frac{\varepsilon_{csm}}{\varepsilon_y} = \left(1 - \frac{0.222}{\bar{\lambda}_p^{\,1.050}}\right)\frac{1}{\bar{\lambda}_p^{\,1.050}}, \qquad \text{for } \bar{\lambda}_p > 0.68 \tag{8}$$

The CSM elastic, linear hardening (bi-linear) material model is illustrated in Fig. 8, in which C_1, C_2, C_3 and C_4 are material coefficients, with the values for various stainless steel grades reported in Table 5 [24]. The material coefficient C_1 is adopted to define a cut-off strain $C_1\varepsilon_u$, to present over-predicting the design failure stress from the employed CSM material model. The coefficient C_2 is utilised in Eq. (9) for the definition of the strain hardening slope E_{sh}, while the predicted ultimate strain ε_u is calculated as $\varepsilon_u=C_3(1-\sigma_{0.2}/\sigma_u)+C_4$.

$$E_{sh} = \frac{f_u - f_y}{C_2\varepsilon_u - \varepsilon_y} \tag{9}$$

Upon calculation of the CSM limiting strain and bi-linear material model, the CSM design stress distribution for cross-sections in bending can be derived, on the basis of the assumption of a linearly-varying strain distribution through the cross-section depth. The resulting CSM bending moment resistance is given by Eq. (10), in which W_{el} and W_{pl} are the elastic and plastic section moduli, respectively, γ_{M0}=1.1 is the partial safety factor for the cross-section capacities of stainless steel elements, and α is the CSM bending coefficient; for SHS and RHS, α is equal to 2.0, while the recommended values for other plated sections (e.g., I-, T-, angle and channel sections) and CHS are summarised in Zhao and Gardner [26]. The CSM was found to result in substantially improved bending moment capacity predictions for non-slender stainless steel SHS and RHS, compared to the plastic and elastic bending moment resistances prescribed in the existing design codes [18,27,28], owing to the consideration of the material strain hardening of stainless steel and the continuous nature of the resistance function.

$$\begin{aligned} M_{csm,Rd} &= \frac{W_{pl}\sigma_{0.2}}{\gamma_{M0}}\left[1+\frac{E_{sh}}{E}\frac{W_{el}}{W_{pl}}\left(\frac{\varepsilon_{csm}}{\varepsilon_y}-1\right)-\left(1-\frac{W_{el}}{W_{pl}}\right)/\left(\frac{\varepsilon_{csm}}{\varepsilon_y}\right)^{\alpha}\right] && \text{for } \bar{\lambda}_p \le 0.68 \\ M_{csm,Rd} &= \frac{\varepsilon_{csm}}{\varepsilon_y}\frac{W_{el}\sigma_{0.2}}{\gamma_{M0}} && \text{for } \bar{\lambda}_p > 0.68 \end{aligned} \tag{10}$$

New interaction factors for stainless steel SHS and RHS beam-columns were then numerically developed based on the revised column buckling strengths and the CSM bending moment capacities as the end points, following the traditional Eurocode derivation procedure for the interaction factors of carbon steel beam-column structural members [3–7]. A comprehensive finite element modelling programme was conducted to derive the failure loads for stainless steel beam-columns with a broad spectrum of member slendernesses under a wide range of loading combinations. The relationship between the new interaction factor k_{csm} and member non-dimensional slenderness $\bar{\lambda}$ for various levels of axial compression $n=N_{Ed}/N_{b,Rd}$ was firstly back-calculated from the numerical results and then transformed into simplified formulae, as given by Eq. (11), in which the values of the coefficients D_1, D_2 and D_3 are set out in Table 6 for each stainless steel grade.

$$k_{csm} = 1 + D_1\left(\bar{\lambda} - D_2\right)n \leq 1 + D_1\left(D_3 - D_2\right)n \tag{11}$$

The proposed design approach was found to yield accurate, consistent and safe-sided strength predictions for stainless steel SHS and RHS beam-columns under uniform bending moment, following comparisons against over 3000 test and FE results [19]. Statistical analyses were also conducted to confirm the reliability of the new beam-column design approach [19].

5.3 New design formulae for stainless steel beam-columns under moment gradients

The proposed design formula for stainless steel SHS and RHS beam-columns under uniform bending moment was shown to yield accurate strength predictions [19], and can thus serve as the basis to develop design rules for beam-columns under moment gradients. A suitable equivalent uniform moment factor is therefore now sought.

The equivalent uniform moment factors adopted in the current SEI/ASCE-8 [27] and AS/NZS 4673 [28] were found to overestimate the beneficial effect of moment gradients on the global stability of beam-columns, and thus led, in some instances, to overestimated beam-column strength predictions. Previous studies [3,5–7,50] on carbon steel beam-columns have acknowledged this point, and suggested the application of a lower limit to the equivalent uniform moment factors C_m for members under high moment gradients. The current EN 1993-1-1 [29] for carbon steel structures adopts the same expression for C_m as SEI/ASCE-8 [27] and AS/NZS 4673 [28], but with a lower limit of 0.4, as given by Eq. (12).

$$C_{m,u} = 0.6 + 0.4\psi \geq 0.4 \tag{12}$$

The proposed design interaction formula for stainless steel SHS and RHS beam-columns under moment gradients therefore constitutes that derived for beam-columns under uniform bending moment, but with the inclusion of the equivalent uniform moment factor from the European code EN 1993-1-1 [29], as given by Eq. (13).

$$\frac{N_{Ed}}{N_{b,Rd}} + C_{m,u} k_{csm} \frac{M_{Ed}}{M_{csm,Rd}} \leq 1 \tag{13}$$

6. Comparisons of predicted beam-column strengths with experimental and numerical data

The accuracy of the new design proposals for stainless steel SHS and RHS beam-columns under moment gradients presented in Section 5 is assessed by means of comparisons against the test results, derived in Section 2, and the FE data, generated from the numerical parametric studies in Section 3. The mean ratios of the test (or FE) capacities to the predicted capacities from the new proposals $N_u/N_{u,Prop}$, as shown in Tables 4(a)–4(c), are equal to 1.07, 1.11 and 1.08, and the corresponding coefficients of the variation (COVs) are equal to 0.04, 0.05 and 0.04 for austenitic, duplex and ferritic stainless steel SHS and RHS beam-columns subjected to moment gradients, respectively. The $N_u/N_{u,Prop}$ ratios are plotted against the end moment ratios ψ, and shown in Figs 4–6 for the three stainless steel grades, respectively. Both the quantitative and graphical evaluation results indicate that the new design proposals for stainless steel SHS and RHS beam-columns under moment gradients generally yield precise and consistent resistance predictions across the full range of end moment ratios from -1.0 to 1.0. Compared to EN 1993-1-4 [18], the proposed approach improves the design accuracy by about 25% and reduces the scatter to only one quarter of that of EN 1993-1-4 [18].

A revised EC3 design method is also proposed by replacing the CSM cross-section bending moment capacity $M_{csm,Rd}$ with the EC3 bending moment resistance (i.e. plastic moment resistance for Class 1 and 2 SHS and RHS and elastic moment resistance for Class 3 cross-sections) in Eq. (13). The corresponding mean test (or numerical) to predicted failure load ratios $N_u/N_{u,EC3,rev.}$ are equal to 1.11, 1.17 and 1.10 for austenitic, duplex and ferritic stainless steel SHS and RHS beam-columns under linearly varying bending moment, respectively, as shown in Table 4(a)–4(c), revealing improved accuracy over the existing EN 1993-1-4 [18] provisions. Also, the corresponding COVs are all 0.05, indicating that the scatter is generally less than one third of that obtained using the current EN 1993-1-4 [18] design rules. The accuracy and consistency of the strength predictions from the revised EC3 approach is also evident in Figs 9(a)–9(c), where the $N_u/N_{u,EC3,rev.}$ ratio is plotted against the end moment ratio ψ.

Comparisons are also made based on the experimental data only, as reported in Table 7. The results of the comparisons indicate that the two proposed design methods yield improved (safe-sided, precise and consistent) strength predictions for stainless steel SHS and RHS beam-columns under moment gradients over the current design standards; this is also evident in Fig. 10, in which the experimental beam-column failure loads are plotted against the predicted failure loads from each design approach.

7. Reliability analysis

Statistical analyses are conducted to assess the reliability of the two new design proposals for stainless steel SHS and RHS beam-columns under moment gradients, according to the procedures and requirements specified in EN 1990 [51]. In the present reliability analyses, the material over-strength ratios for austenitic, duplex and ferritic stainless steels were respectively taken as 1.3, 1.1 and 1.2, with COVs of 0.060, 0.030 and 0.045, while the COV of the stainless steel cross-section geometric properties was equal to 0.050 [52]. Table 8 reports the key calculated statistical parameters for the two new proposed beam-column design approaches, including the design fractile factor $k_{d,n}$, the mean ratio of experimental and FE capacities to design model capacities b, the COV of the experiments and numerical simulations relative to the resistance model V_δ, the COV incorporating the uncertainties of model and basic variables V_r and the partial factor for member global buckling strength γ_{M1}. The resulting partial safety factors for both of the two new beam-column design approaches, as reported in Tables 8(a) and 8(b), are less than 1.1 – the value of the partial factor utilised in the current EN 1993-1-4 [18], therefore confirming the reliability of the two new design proposals for stainless steel SHS and RHS beam-columns under moment gradients.

8. Conclusions

Existing design rules for stainless steel SHS and RHS beam-columns under moment gradients, given in EN 1993-1-4 [18], SEI/ASCE-8 [27] and AS/NZS 4673 [28], were developed through the employment of the corresponding design interaction formulae for beam-column members under uniform bending moment, but with the use of an equivalent uniform moment factor to account for the favourable effect of non-uniform bending moment distributions on member stability. However, previous experimental studies on stainless steel beam-columns [12,14,15,19] have revealed that both the codified design interaction curves for beam-columns under uniform bending moment and the adopted equivalent uniform moment factors have some shortcomings. This, in turn, leads to inaccurate strength predictions for beam-columns under moment gradients. Improved design approaches have therefore been developed, firstly through the derivation of more accurate design interaction curves for beam-columns under uniform bending moment and then through the employment of more suitable equivalent uniform moment factors. The new design proposals were shown to provide safe-sided, accurate and consistent strength predictions through comparisons against experimental and numerical results. Finally, statistical analyses were performed to demonstrate the reliability of the new design approaches, according to the requirements specified in EN 1990 [51].

References

[1] Trahair NS, Bradford MA, Nethercot DA, Gardner L. The behaviour and design of steel structures to EC3. CRC Press, 2007.

[2] Lindner J. Design of steel beams and beam columns. Engineering Structures, 1997;19(5): 378–84.

[3] Boissonnade N, Jaspart J-P, Muzeau J-P, Villette M. Improvement of the interaction formulae for beam columns in Eurocode 3. Computers & Structures, 2002;80(27):2375–85.

[4] Lindner J. Design of beams and beam columns. Progress in Structural Engineering and Materials, 2003;5(1):38–47.

[5] Boissonnade N, Jaspart J-P, Muzeau J-P, Villette M. New interaction formulae for beam-columns in Eurocode 3: the French–Belgian approach. Journal of Constructional Steel Research, 2004;60(3):421–31.

[6] Boissonnade N, Greiner R, Jaspart J-P, Lindner J. Rules for Member Stability in EN 1993-1-1: Background documentation and design guidelines. ECCS European Convention for Constructional Steelwork, 2006.

[7] Greiner R, Lindner J. Interaction formulae for members subjected to bending and axial compression in EUROCODE 3 – the Method 2 approach. Journal of Constructional Steel Research, 2006;62(8):757–70.

[8] Ziemian RD. Guide to Stability Design Criteria for Metal Structures, Sixth Editions. John Wiley & Sons, Inc., New York, USA, 2010.

[9] Talja A, Salmi P. Design of stainless steel RHS beams, columns and beam-columns. Technical Research Centre of Finland, Finland; 1995.

[10] Lui WM, Ashraf M, Young B. Tests of cold-formed duplex stainless steel SHS beam–columns. Engineering Structures, 2014;74:111–21.

[11] Huang Y, Young B. Experimental investigation of cold-formed lean duplex stainless steel beam-columns. Thin-Walled Structures, 2014;76:105–17.

[12] Zhao O, Gardner L, Young B. Buckling of ferritic stainless steel members under combined axial compression and bending. Journal of Constructional Steel Research, 2016;117:35–48.

[13] Arrayago I, Real E, Mirambell E. Experimental study on ferritic stainless steel RHS and SHS beam-columns. Thin-Walled Structures, 2016;100:93–104.

[14] Zhao O, Gardner L, Young B. Testing and numerical modelling of austenitic stainless steel CHS beam-columns. Engineering Structures, 2016;111:263–74.

[15] Zhao O, Gardner L, Young B. Experimental Study of Ferritic Stainless Steel Tubular Beam-Column Members Subjected to Unequal End Moments. Journal of Structural Engineering (ASCE), 2016;142(11):04016091.

[16] Greiner R, Kettler M. Interaction of bending and axial compression of stainless steel members. Journal of Constructional Steel Research, 2008;64(11):1217–24.

[17] Lopes N, Vila Real P, Simões da Silva L. Stainless steel beam-columns interaction curves with and without lateral torsional buckling. In: Proceedings of the 7th EUROMECH Solid Mechanics Conference, Lisbon, Portugal; 2009.

[18] EN 1993-1-4:2006+A1:2015. Eurocode 3: Design of steel structures – Part 1.4: General rules – Supplementary rules for stainless steels, including amendment A1 (2015). Brussels: European Committee for Standardization (CEN); 2015.

[19] Zhao O, Gardner L, Young B. Behaviour and design of stainless steel SHS and RHS beam-columns. Thin-Walled Structures, 2016;106:330–45.

[20] Buchanan L, Gardner L, Zhao O, Real E. Design of stainless steel CHS beam-columns. In: Proceedings of the 16th International Symposium on Tubular Structures, Australia; 2017.

[21] Afshan S, Zhao O, Gardner L. Standardised material properties for numerical parametric studies of stainless steel structures and buckling curves for tubular columns. Journal of Constructional Steel Research, https://doi.org/10.1016/j.jcsr.2018.02.019.

[22] Gardner L. The Continuous Strength Method. Proceedings of the Institution of Civil Engineers – Structures and Buildings, 2008;161(3):127–33.

[23] Afshan S, Gardner L. The continuous strength method for structural stainless steel design. Thin-Walled Structures, 2013;68(4):42–49.

[24] Buchanan C, Gardner L, Liew A. The continuous strength method for the design of circular hollow sections. Journal of Constructional Steel Research, 2016;118:207–16.

[25] Zhao O, Afshan S, Gardner L. Structural response and continuous strength method design of slender stainless steel cross-sections. Engineering Structures, 2017;140:14–25.

[26] Zhao O, Gardner L. The continuous strength method for the design of mono-symmetric and asymmetric stainless steel cross-sections in bending. Journal of Constructional Steel Research, 2018;150:141–152.

[27] SEI/ASCE 8-02. Specification for the design of cold-formed stainless steel structural members. Reston: American Society of Civil Engineers (ASCE); 2002.

[28] AS/NZS 4673. Cold-formed stainless steel structures. Sydney: AS/NZS 4673:2001; 2001.

[29] EN 1993-1-1. Eurocode 3: Design of steel structures – Part 1.1: General rules and rules for buildings. Brussels: European Committee for Standardization (CEN); 2005.

[30] Hibbitt, Karlsson & Sorensen, Inc. ABAQUS. ABAQUS/Standard user's manual volumes I-III and ABAQUS CAE manual. Version 6.12. Pawtucket (USA); 2012.

[31] Gardner L, Nethercot DA. Numerical modeling of stainless steel structural components – A consistent approach. Journal of Structural Engineering (ASCE), 2004;130(10):1586–601.

[32] Zhao O, Rossi B, Gardner L, Young B. Behaviour of structural stainless steel cross-sections under combined loading – Part II: Numerical modelling and design approach. Engineering Structures, 2015;89:247–59.

[33] Zhao O, Rossi B, Gardner L, Young B. Experimental and numerical studies of ferritic stainless steel tubular cross-sections under combined compression and bending. Journal of Structural Engineering (ASCE), 2016;142(2):04015110.

[34] Zhao O, Gardner L, Young B. Structural performance of stainless steel circular hollow sections under combined axial load and bending – Part 2: Parametric studies and design. Thin-Walled Structures, 2016;101:240–48.

[35] Cruise RB, Gardner L. Strength enhancements induced during cold forming of stainless steel sections. Journal of Constructional Steel Research, 2008;64(11):1310–6.

[36] Rasmussen KJR, Hancock GJ. Design of cold-formed stainless steel tubular members. I: Columns. Journal of Structural Engineering (ASCE), 1993;119(8):2349–67.

[37] Cruise RB, Gardner L. Residual stress analysis of structural stainless steel sections. Journal of Constructional Steel Research, 2008;64(3):352–66.

[38] Jandera M, Gardner L, Machacek J. Residual stresses in cold-rolled stainless steel hollow sections. Journal of Constructional Steel Research, 2008;64(11):1255–63.

[39] Dawson RG, Walker AC. Post-buckling of geometrically imperfect plates. Journal of the Structural Division (ASCE), 1972;98(1):75–94.

[40] Zhao O, Rossi B, Gardner L, Young, B. Behaviour of structural stainless steel cross-sections under combined loading – Part I: Experimental study. Engineering Structures, 2015;89:236–46.

[41] Ramberg W, Osgood WR. Description of stress–strain curves by three parameters. Technical note No 902, Washington DC: National advisory committee for aeronautics; 1943.

[42] Hill HN. Determination of stress–strain relations from offset yield strength values. Technical note No 927, Washington DC: National advisory committee for aeronautics; 1944.

[43] Mirambell E, Real E. On the calculation of deflections in structural stainless steel beams: An experimental and numerical investigation. Journal of Constructional Steel Research, 2000;54(1):109–33.

[44] Rasmussen KJR. Full-range stress-strain curves for stainless steel alloys. Journal of Constructional Steel Research, 2003;59(1):47–61.

[45] Gardner L, Ashraf M. Structural design for non-linear metallic materials. Engineering Structures, 2006;28(6):926–34.

[46] Rasmussen KJR, Rondal J. Strength curves for metal columns. Journal of Structural Engineering (ASCE), 1997;123(6):721–8.

[47] Zheng B, Shu G, Xin L, Yang R, Jiang Q. Study on the Bending Capacity of Cold-formed Stainless Steel Hollow Sections. Structures, 2016;8:63–74.

[48] Huang Y, Young B. Experimental and numerical investigation of cold-formed lean duplex stainless steel flexural members. Thin-Walled Structures, 2013;73:216–28.

[49] Schafer BW, Ádány S. Buckling analysis of cold-formed steel members using CUFSM: conventional and constrained finite strip methods. In: Proceedings of the eighteenth international specialty conference on cold-formed steel structures, Orlando, USA; 2006. p. 39–54.

[50] Austin WJ. Strength and design of metal beam-columns. Journal of the Structural Division, 1961;87(4):1–34.

[51] EN 1990. Eurocode – basis of structural design. Brussels: European Committee for Standardization (CEN); 2002.

[52] Afshan S, Francis P, Baddoo NR, Gardner L. Reliability analysis of structural stainless steel design provisions. Journal of Constructional Steel Research, 2015;114:293–304.

Table 1 Summary of experimental results on stainless steel SHS and RHS beam-columns under moment gradients [15].

Test series	Specimen ID	L_{cr} (mm)	$\bar{\lambda}$	e_0 (mm)	ψ	$N_{u,test}$ (kN)	$M_{u,b}$ (kNm)	$M_{u,t}$ (kNm)
RHS 100×40×2-MI-500	1A	674.8	0.52	20.6	-0.59	101.3	2.09	-1.23
	1B	674.8	0.52	20.6	-0.22	96.2	1.98	-0.44
	1C	674.8	0.52	19.6	-0.11	104.0	2.04	-0.22
	1D	674.8	0.52	19.5	0.23	95.9	1.87	0.43
	1E	674.8	0.52	19.6	0.70	88.7	1.74	1.22
	1F	674.8	0.52	20.3	1.00	77.6	1.58	1.58
RHS 100×40×2-MI-1250	2A	1424.8	1.09	19.8	-0.71	82.2	1.63	-1.16
	2B	1424.8	1.09	19.9	-0.35	76.2	1.52	-0.53
	2C	1424.8	1.09	20.0	0.07	66.5	1.33	0.09
	2D	1424.8	1.09	19.8	0.31	66.3	1.31	0.41
	2E	1424.8	1.09	20.2	0.75	62.2	1.26	0.94
	2F	1424.8	1.08	19.7	1.00	55.5	1.09	1.09
SHS 60×60×3-600	3A	774.8	0.54	19.3	-0.66	203.0	3.92	-2.59
	3B	774.8	0.54	20.7	-0.26	188.3	3.90	-1.01
	3C	774.8	0.54	20.0	-0.03	182.9	3.66	-0.11
	3D	774.8	0.54	20.1	0.31	172.1	3.46	1.07
	3E	774.8	0.54	20.3	0.75	158.2	3.21	2.41
	3F	774.8	0.54	19.8	1.00	150.4	2.98	2.98
SHS 60×60×3-1200	4A	1374.8	0.95	20.6	-0.80	164.5	3.39	-2.71
	4B	1374.8	0.96	19.2	-0.40	146.1	2.81	-1.12
	4C	1374.8	0.96	20.6	-0.03	135.8	2.80	-0.08
	4D	1374.8	0.95	18.8	0.32	130.8	2.46	0.79
	4E	1374.8	0.96	20.3	0.75	116.9	2.37	1.78
	4F	1374.8	0.96	19.0	1.00	112.3	2.13	2.13

Table 2 Comparison of numerical failure loads with experimental failure loads for various combinations of local and global imperfection amplitudes.

Test series	Specimen ID	Finite element N_u/Test N_u					
		$\omega_g+\omega_0$	$L_{cr}/1000+\omega_0$	$L_{cr}/1500+\omega_0$	$\omega_g+\omega_{D\&W}$	$L_{cr}/1000+\omega_{D\&W}$	$L_{cr}/1500+\omega_{D\&W}$
RHS 100×40×2-MI-500	1A	0.97	0.95	0.96	0.96	0.95	0.95
	1B	0.95	0.94	0.95	0.94	0.94	0.94
	1C	0.95	0.95	0.95	0.94	0.94	0.94
	1D	0.99	0.98	0.98	0.98	0.98	0.98
	1E	0.95	0.94	0.94	0.95	0.94	0.94
	1F	0.93	0.92	0.93	0.93	0.92	0.92
RHS 100×40×2-MI-1250	2A	0.96	0.93	0.95	0.95	0.93	0.94
	2B	0.94	0.92	0.93	0.93	0.91	0.92
	2C	0.97	0.95	0.96	0.96	0.94	0.95
	2D	0.92	0.90	0.91	0.91	0.90	0.91
	2E	0.90	0.89	0.90	0.90	0.89	0.90
	2F	0.93	0.91	0.92	0.92	0.90	0.91
SHS 60×60×3-600	3A	1.03	1.03	1.03	1.03	1.03	1.03
	3B	1.03	1.02	1.02	1.03	1.02	1.02
	3C	1.03	1.02	1.03	1.03	1.02	1.03
	3D	1.03	1.02	1.03	1.03	1.02	1.03
	3E	1.03	1.02	1.02	1.03	1.02	1.02
	3F	1.04	1.03	1.03	1.04	1.03	1.03
SHS 60×60×3-1200	4A	1.01	0.99	1.00	1.01	0.99	1.00
	4B	1.04	1.02	1.03	1.04	1.02	1.03
	4C	1.01	0.99	1.00	1.01	0.99	1.00
	4D	1.00	0.98	0.99	1.00	0.98	0.99
	4E	1.00	0.99	1.00	1.00	0.99	1.00
	4F	1.02	1.01	1.01	1.02	1.01	1.01
Mean		0.98	0.97	0.98	0.98	0.97	0.98
COV		0.04	0.05	0.04	0.05	0.04	0.05

Table 3 Summary of flat and corner material properties utilised in the numerical models.

(a) Flat material properties.

Material grade	E	$\sigma_{0.2}$	$\sigma_{1.0}$	σ_u	R-O coefficient		
	(GPa)	(MPa)	(MPa)	(MPa)	n	$n'_{0.2,1.0}$	$n'_{0.2,u}$
Austenitic	196	335	384	608	5.9	2.6	3.5
Duplex	198	635	694	756	6.0	3.2	4.2
Ferritic	199	470	485	488	7.3	7.6	10.9

(b) Corner material properties.

Material grade	E	$\sigma_{0.2}$	$\sigma_{1.0}$	σ_u	R-O coefficient		
	(GPa)	(MPa)	(MPa)	(MPa)	n	$n'_{0.2,1.0}$	$n'_{0.2,u}$
Austenitic	201	559	622	725	4.8	3.9	4.1
Duplex	207	833	1053	1079	5.0	4.5	6.1
Ferritic	200	579	–	648	4.0	–	7.3

Table 4 Comparison of test and FE beam-column strengths with predicted strengths.

(a) Austenitic stainless steel.

No. of tests: 0 No. of FE modelling: 500	$N_u/N_{u,EC3}$	$N_u/N_{u,ASCE}$	$N_u/N_{u,AS/NZS}$	$N_u/N_{u,Prop}$	$N_u/N_{u,EC3,rev.}$
Mean	1.30	1.01	1.13	1.07	1.11
COV	0.16	0.05	0.05	0.04	0.05

(b) Duplex stainless steel.

No. of tests: 0 No. of FE modelling: 500	$N_u/N_{u,EC3}$	$N_u/N_{u,ASCE}$	$N_u/N_{u,AS/NZS}$	$N_u/N_{u,Prop}$	$N_u/N_{u,EC3,rev.}$
Mean	1.45	1.06	1.12	1.11	1.17
COV	0.16	0.05	0.04	0.05	0.05

(c) Ferritic stainless steel.

No. of tests: 12 No. of FE modelling: 500	$N_u/N_{u,EC3}$	$N_u/N_{u,ASCE}$	$N_u/N_{u,AS/NZS}$	$N_u/N_{u,Prop}$	$N_u/N_{u,EC3,rev.}$
Mean	1.33	1.01	1.08	1.08	1.10
COV	0.17	0.04	0.04	0.04	0.05

Table 5 Summary of the CSM material model coefficients for stainless steels.

Grade	C_1	C_2	C_3	C_4
Austenitic	0.10	0.16	1.00	0
Duplex	0.10	0.16	1.00	0
Ferritic	0.40	0.45	0.60	0

Table 6 Proposed coefficients for interaction factors (Eq. (11)) for different stainless steel grades.

Grade	D_1	D_2	D_3
Austenitic	2.0	0.30	1.3
Duplex	1.5	0.40	1.4
Ferritic	1.3	0.45	1.6

Table 7 Comparison of experimental beam-column strengths with predicted strengths.

No. of tests: 12	$N_{u,test}/N_{u,EC3}$	$N_{u,test}/N_{u,ASCE}$	$N_{u,test}/N_{u,AS/NZS}$	$N_{u,test}/N_{u,Prop}$	$N_{u,test}/N_{u,EC3,rev.}$
Mean	1.26	1.03	1.12	1.07	1.08
COV	0.13	0.03	0.03	0.04	0.04

Table 8 Reliability analysis results calculated according to EN 1990.

(a) Proposed design method

Grade	No. of tests and FE simulations	$k_{d,n}$	b	V_δ	V_r	γ_{M1}
Austenitic	500	3.110	1.046	0.045	0.090	0.97
Duplex	500	3.110	1.110	0.058	0.082	1.06
Ferritic	512	3.109	1.078	0.045	0.081	0.99

(b) Revised EC3 design approach

Grade	No. of tests and FE simulations	$k_{d,n}$	b	V_δ	V_r	γ_{M1}
Austenitic	500	3.110	1.083	0.047	0.091	0.94
Duplex	500	3.110	1.155	0.054	0.079	1.01
Ferritic	512	3.109	1.090	0.044	0.081	0.98

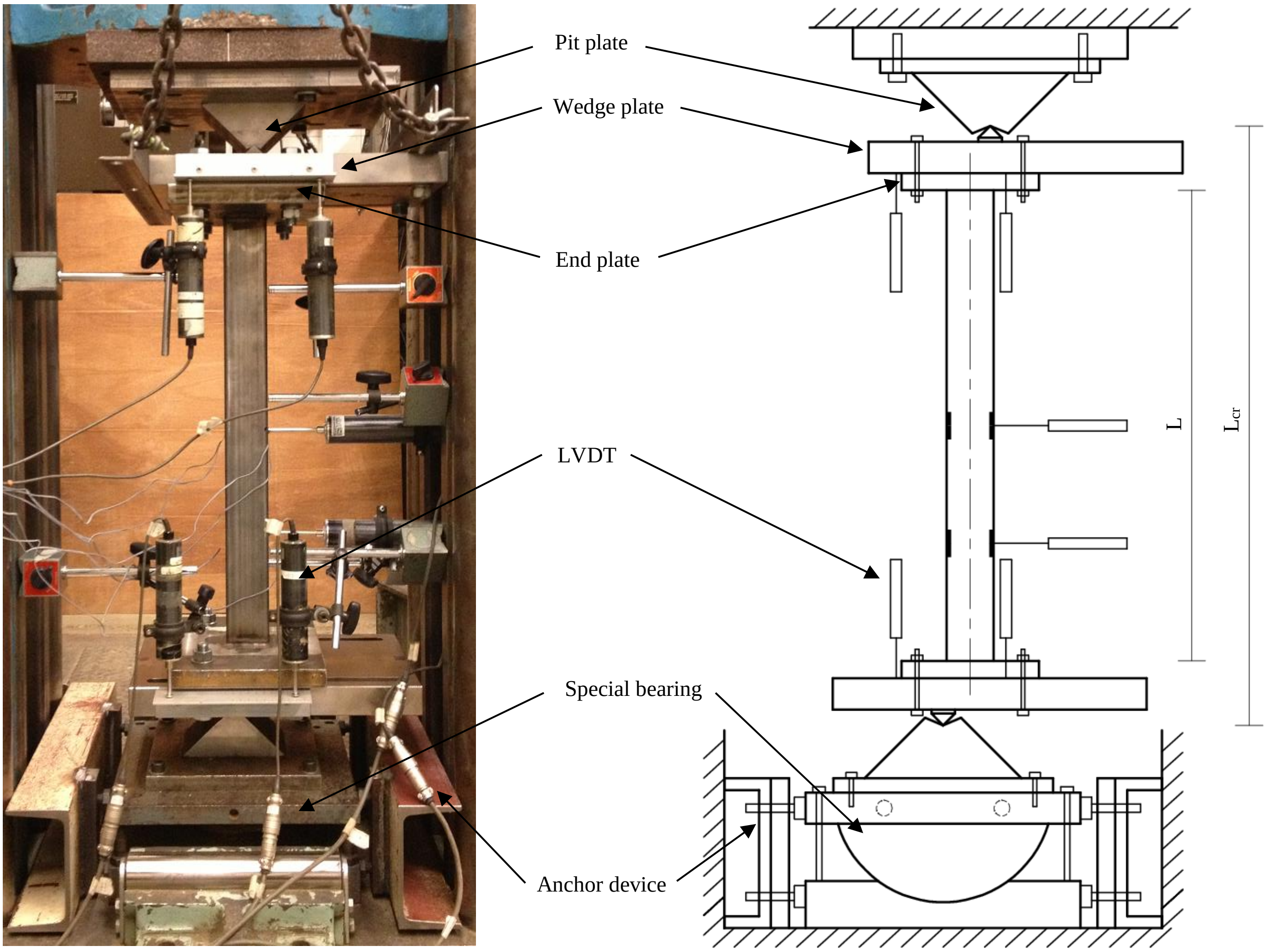

(a) Experimental setup.

(b) Schematic diagram of the test setup.

Fig. 1. Beam-column test configuration [15].

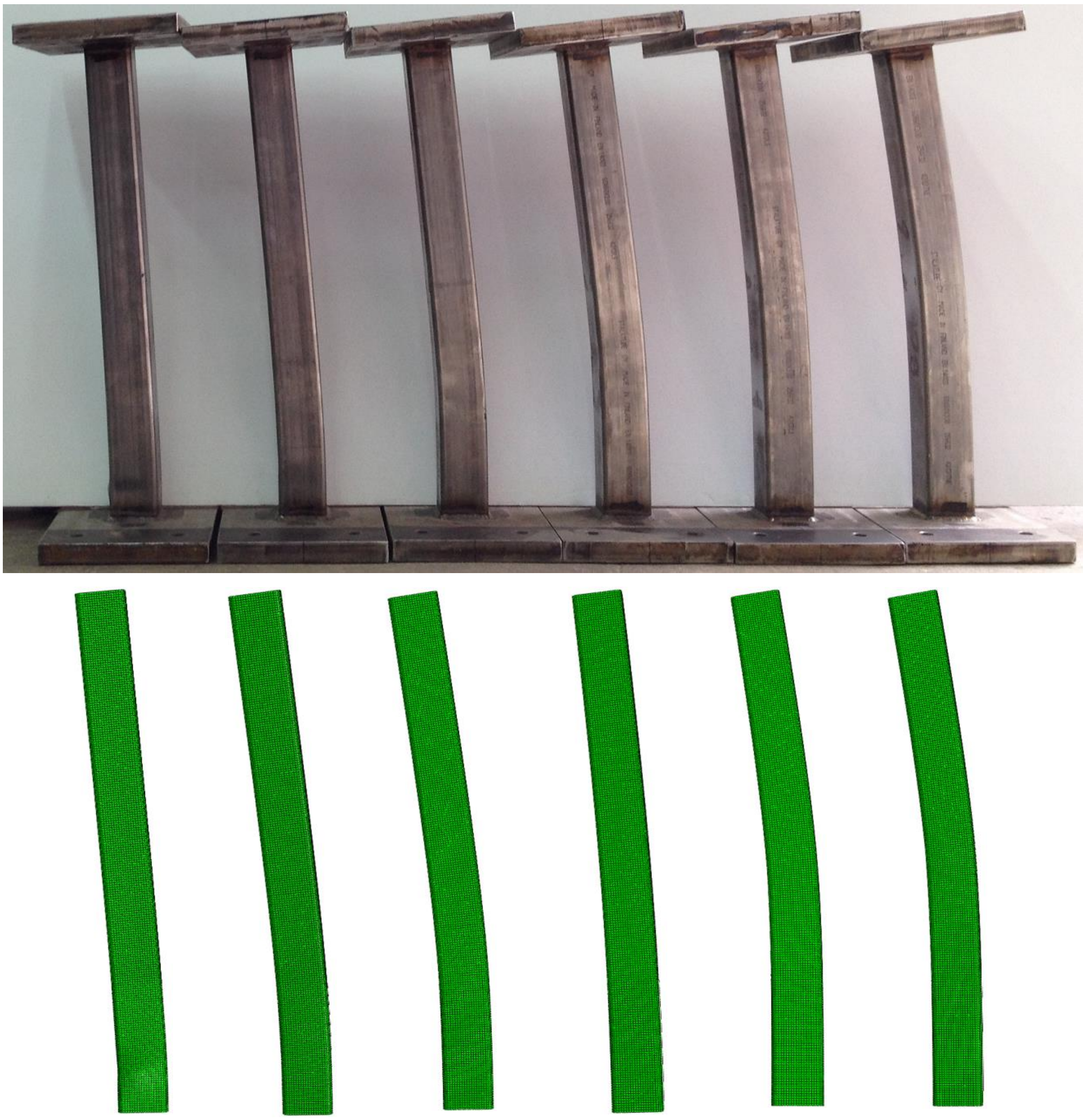

Fig. 2. Experimental (top) and numerical (bottom) failure modes for SHS 60×60×3-600 specimens [15]; from left to right, the end moment ratios ψ are equal to -0.66, -0.26, -0.03, 0.31, 0.75 and 1.00, respectively.

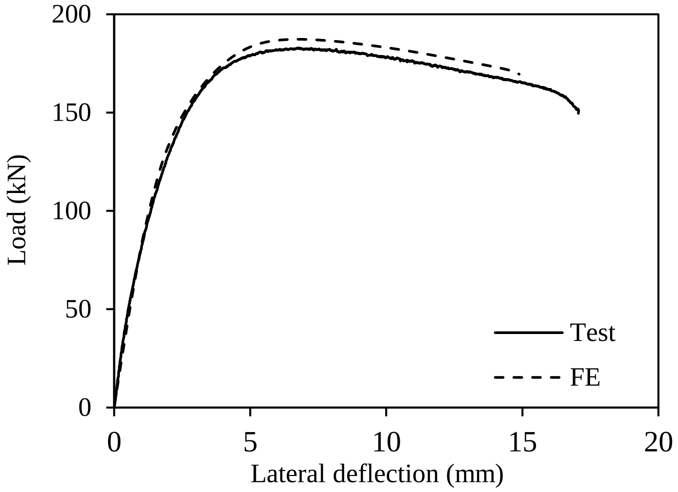

(a) At mid-height

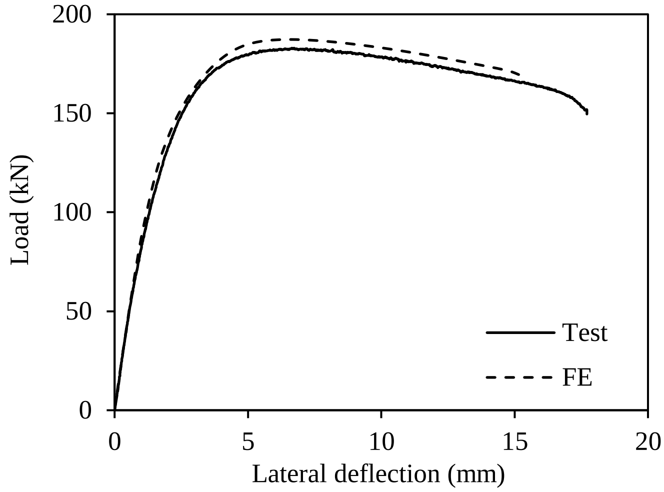

(b) At quarter-height

Fig. 3. Experimental and numerical load–lateral deflection curves for beam-column specimen SHS 60×60×3-600-3C [15] (e_0=20.0 mm, ψ=-0.03).

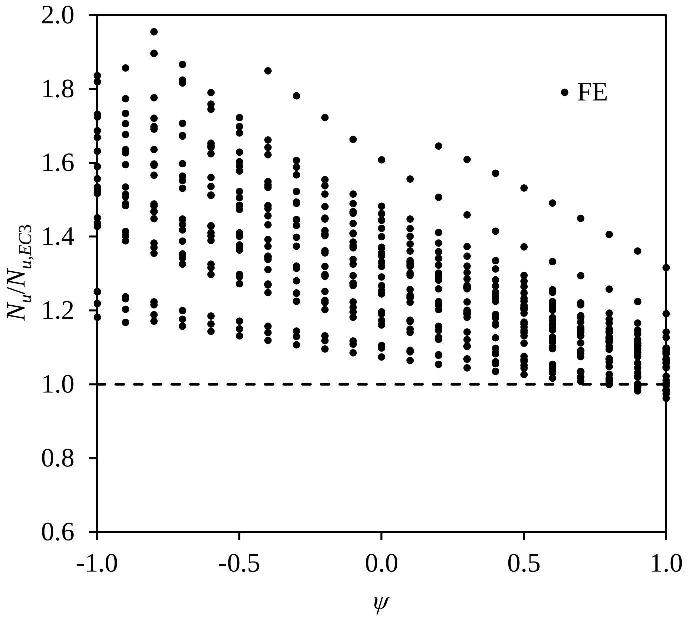

(a) EN 1993-1-4.

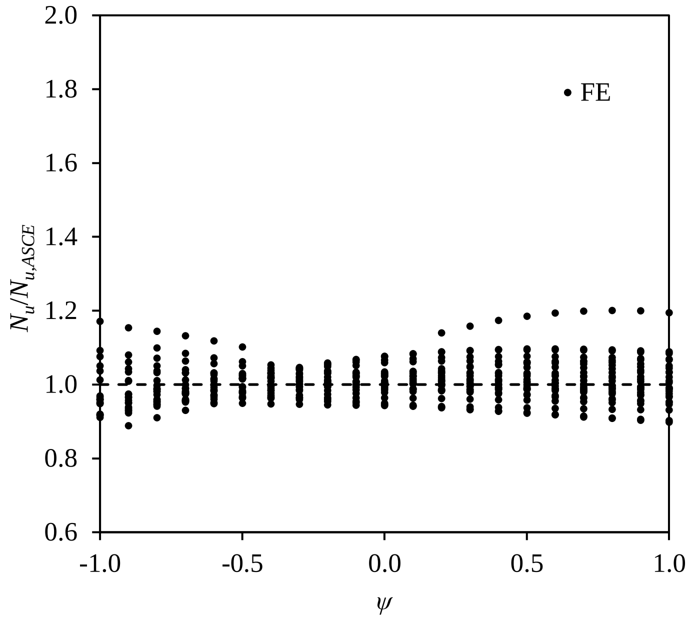

(b) SEI/ASCE-8.

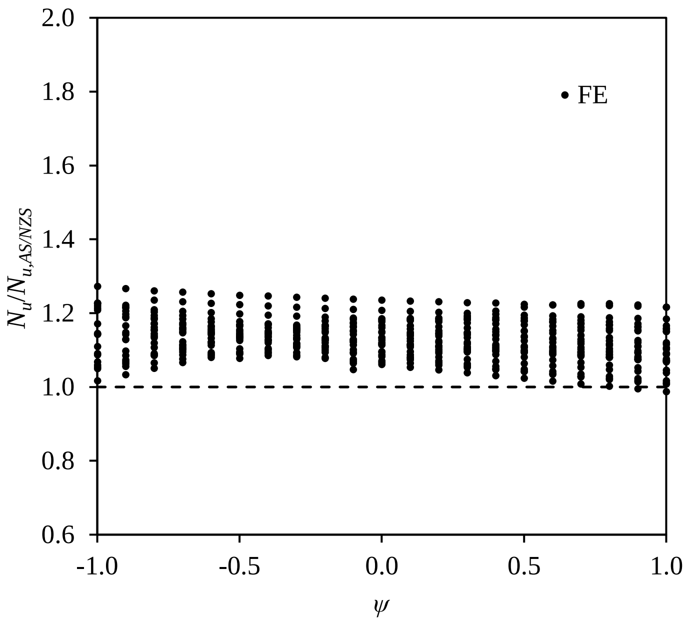

(c) AS/NZS 4673.

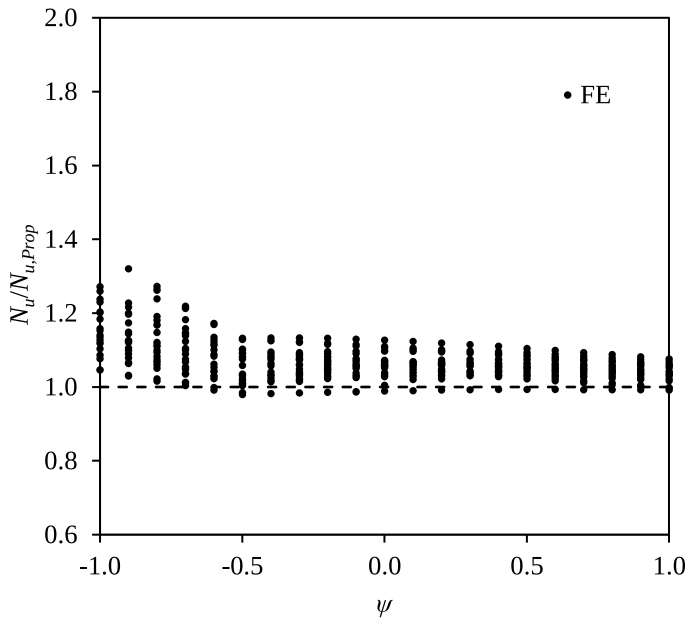

(d) Proposed approach.

Fig. 4. Comparison of austenitic stainless steel beam-column test and FE results with predicted strengths.

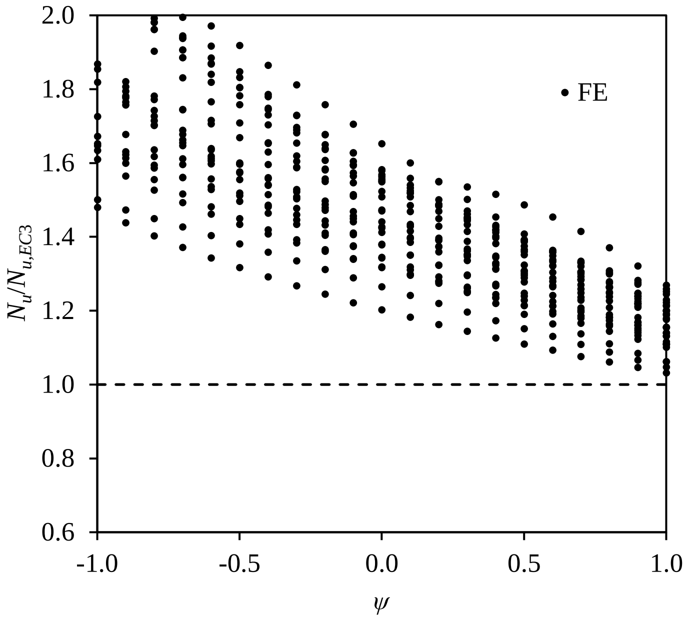

(a) EN 1993-1-4.

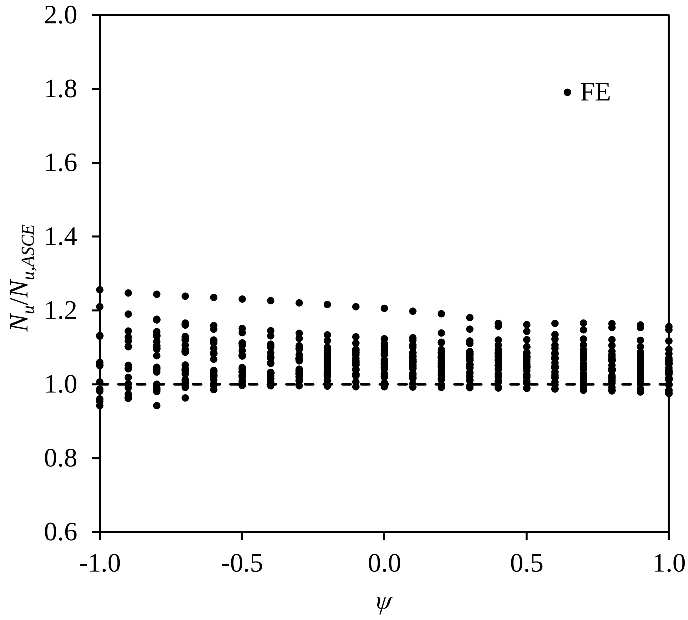

(b) SEI/ASCE-8.

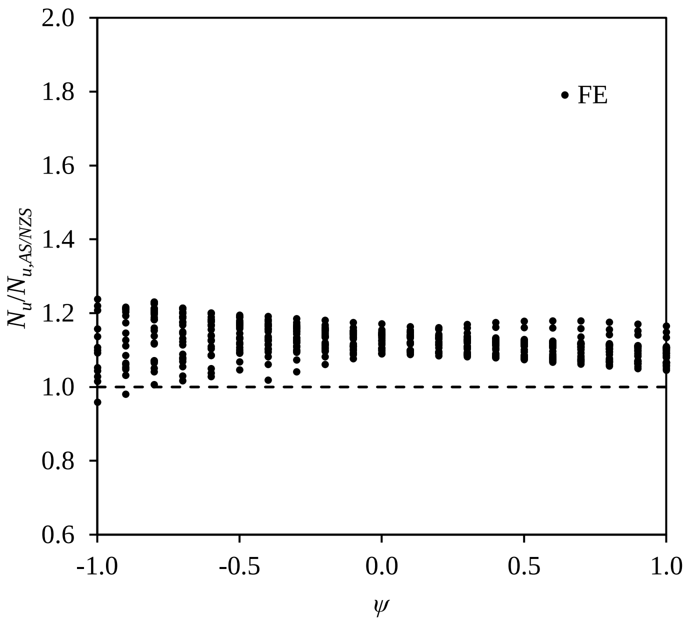

(c) AS/NZS 4673.

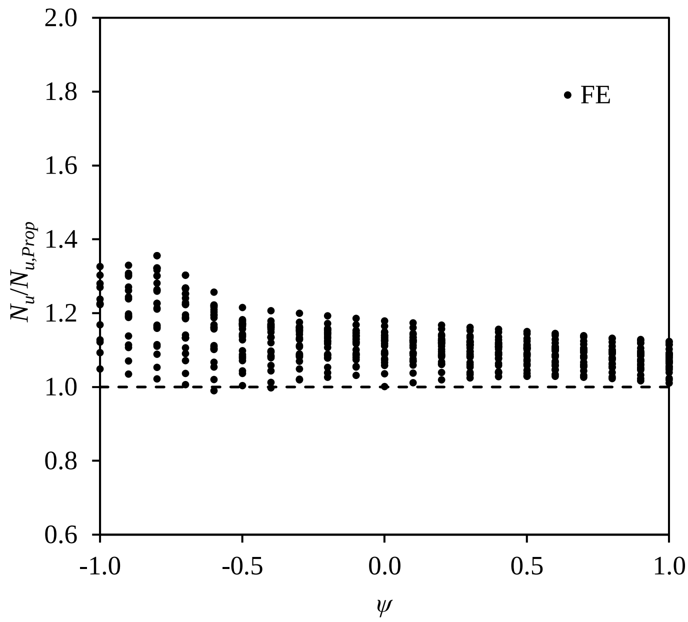

(d) Proposed approach.

Fig. 5. Comparison of duplex stainless steel beam-column test and FE results with predicted strengths.

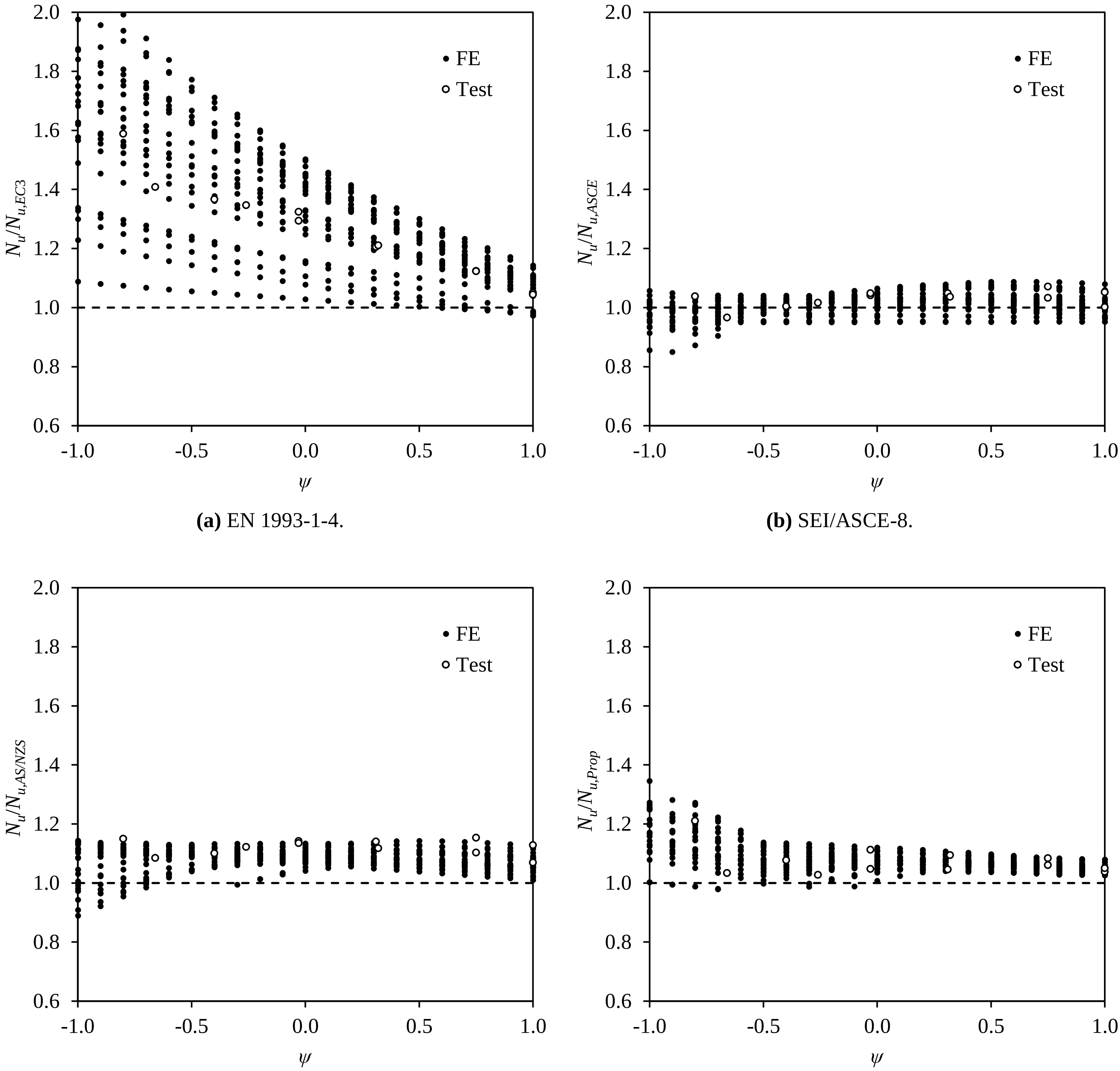

(a) EN 1993-1-4.

(b) SEI/ASCE-8.

(c) AS/NZS 4673.

(d) Proposed approach.

Fig. 6. Comparison of ferritic stainless steel beam-column test and FE results with predicted strengths.

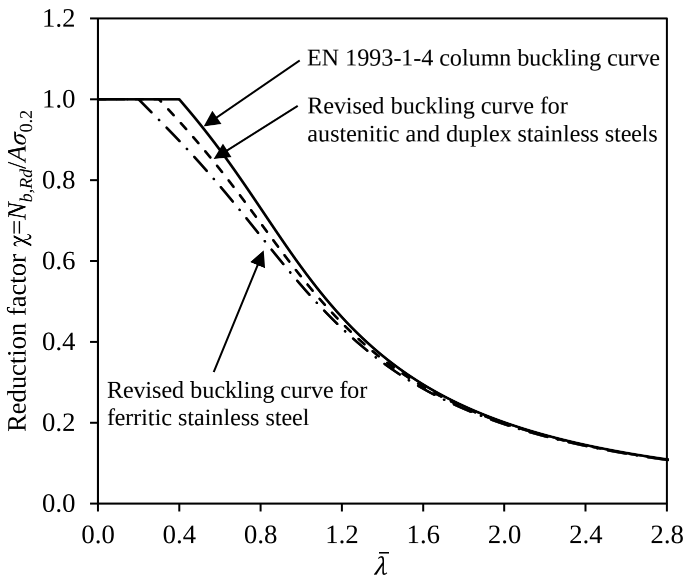

Fig. 7. Comparisons between the EN 1993-1-4 and revised column buckling curves for cold-formed stainless steel SHS and RHS.

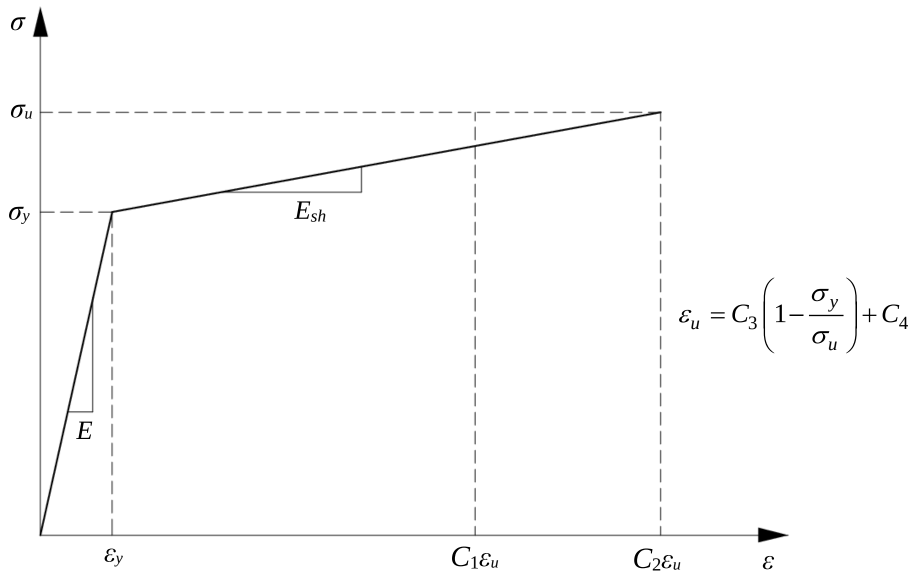

Fig. 8. CSM elastic, linear hardening material model.

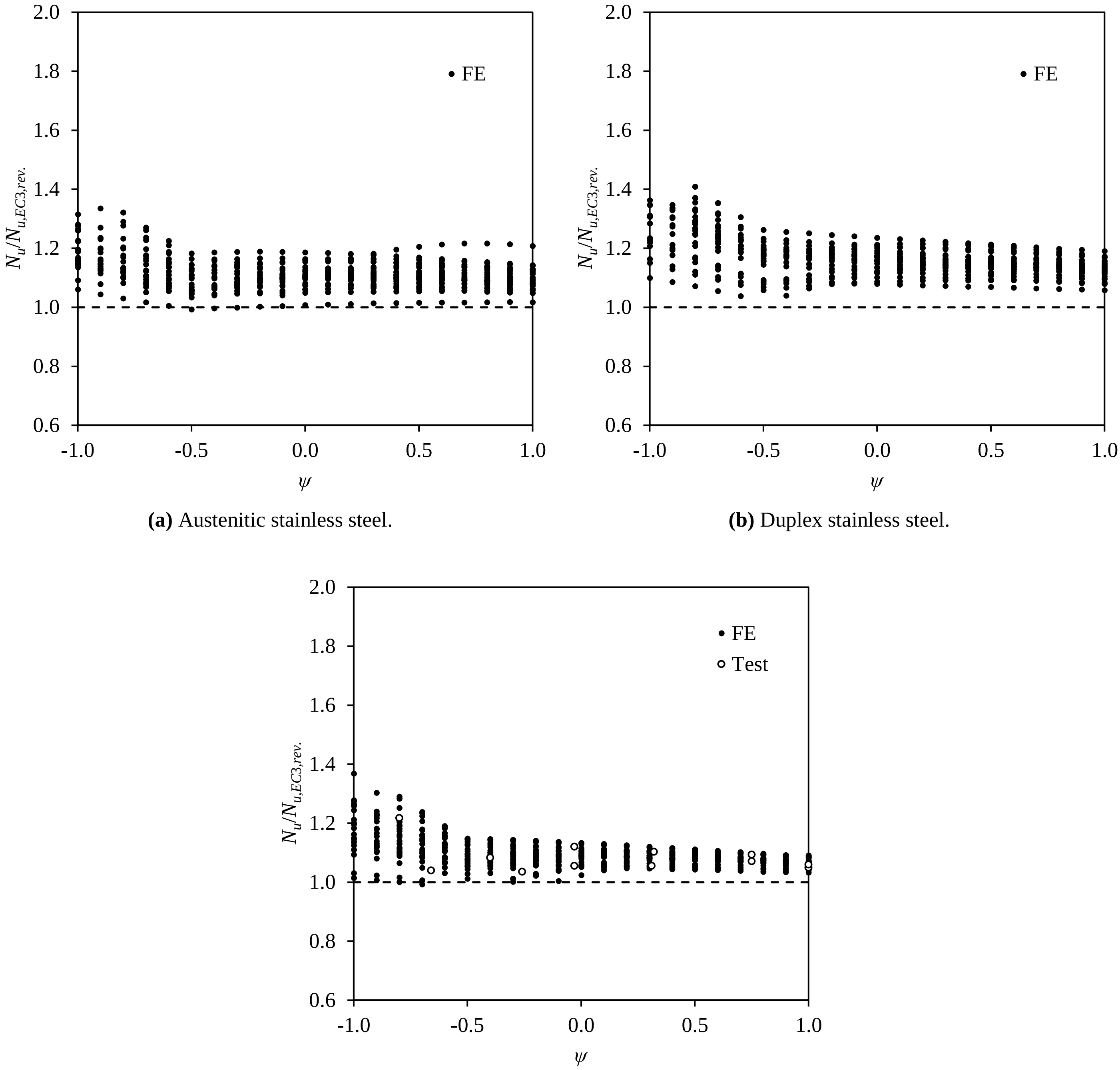

(a) Austenitic stainless steel.

(b) Duplex stainless steel.

(c) Ferritic stainless steel.

Fig. 9. Comparisons of stainless steel beam-column test and FE results with predicted strengths from the revised EC3 approach.

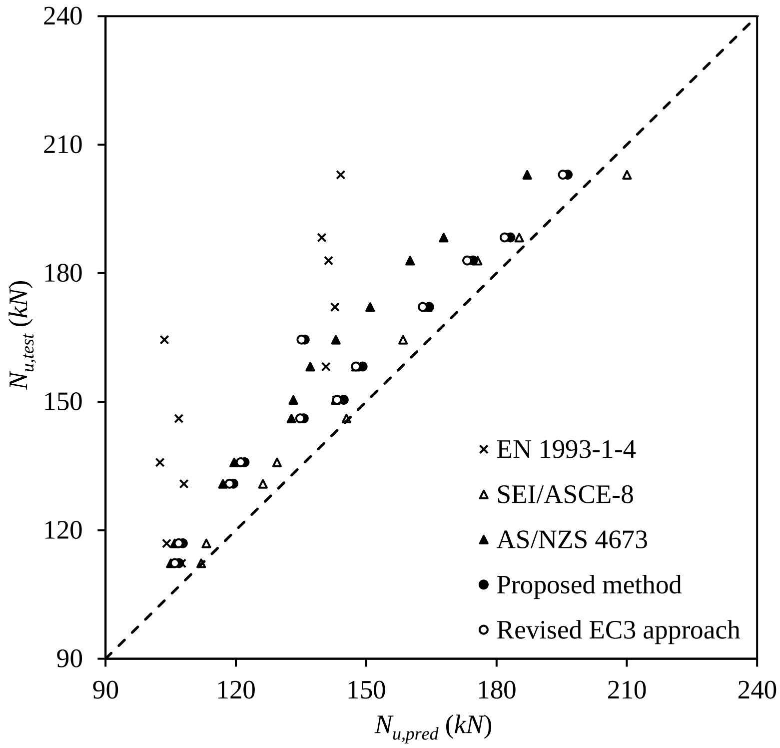

Fig. 10. Comparison of ferritic stainless steel beam-column test results with predicted strengths.